REVIEW PAPER

Recent advances of phase engineering in group VI transition metal dichalcogenides

Lingjia Meng[1,2] · Yang Ma[2] · Kunpeng Si[2] · Shiyu Xu[2] · Jinliang Wang[1] · Yongji Gong[2]

Abstract

As the crystal quality and phase structure of two-dimensional (2D) transition metal dichalcogenides (TMDs) have significant impacts on their properties such as electroconductivity, superconductivity and chemical stability, the precise synthesis, which plays an important role in fundamental researches and industrial applications, is highly required. Group VI TMDs, such as MoS_2, usually exhibit diverse polymorphs including semiconducting 1H and metallic 1T phases. Even great efforts are devoted to revealing the structure-dependent physicochemical nature of TMDs by modulating their phases from the stable to the metastable at the atomic scale, there are still challenges on the phase-controlled synthesis of Group VI TMDs with metallic or semimetal properties. In this review, methods such as ion intercalation, chemical doping, strain engineering, defect triggering, and electric-field treatment are examined in detail. Finally, challenges and opportunities in this research field are proposed.

Keywords Phase transition engineering · Transition metal dichalcogenides · Two-dimensional materials · Molybdenum disulfide · Tungsten disulfide

1 Introduction

Beyond intensive studies focused on graphene-related materials, recently, there has been strong interest in two-dimensional TMDs, whose various properties are highly sensitive to the crystal structures [1–4]. The emerging TMDs with phase-related properties make them attractive to fundamental studies of physicochemical phenomena such as electronics, strong spin-orbit coupling and energy harvesting at the nanoscale [5–9]. Despite the promising outlooks, the phase-controlled synthesis of TMDs is technically challenging, as the novel performance is usually related to the metastable state of crystal structure. Meanwhile, the mechanisms behind the phase-dependent nature deserve deeper understanding and further exploration.

✉ Jinliang Wang
   wangjinliang@buaa.edu.cn

✉ Yongji Gong
   yongjigong@buaa.edu.cn

[1] School of Physics and Nuclear Engineering, Beihang University, Beijing 100191, China

[2] School of Materials Science and Engineering, Beihang University, Beijing 100191, China
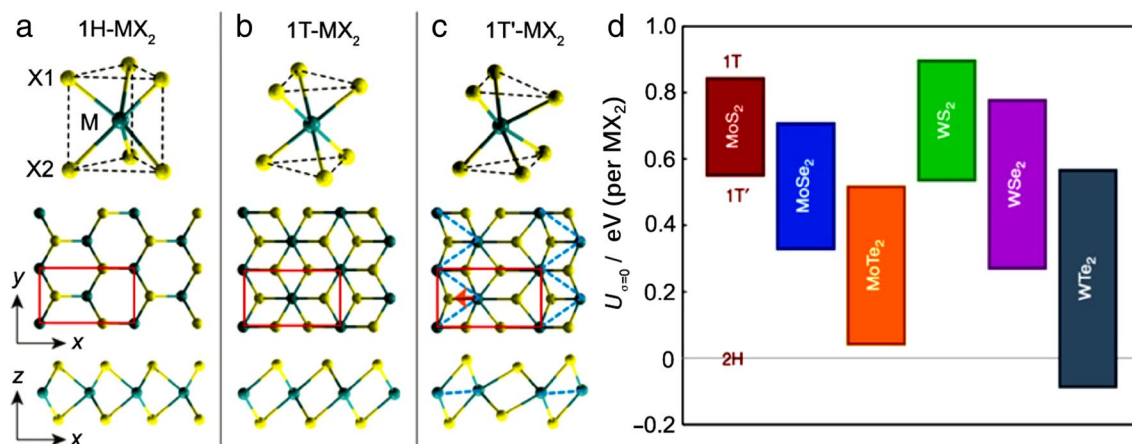
TMDs are layered inorganic compounds with strong lateral chemical bonding but relatively weak van der Waals interlayer bonding [10–14], so that the mono- and few-layer TMDs nanosheets can be easily isolated due to the weak interlayer forces [13, 15–17]. Different from graphene, each Group VI TMD single layer exhibits the "sandwich" structure, hence they can be presented with a general chemical formula MX_2 (M stands for W and Mo, and X stands for Te, Se and S) [18]. The electronic structure of monolayer TMDs depends on the electron numbers in d orbitals of the transition metals [19–25], thus various phases can be realized by tuning the combination state between transition metals and chalcogen atoms in a single-layered system. Generally, there are two common types of phase structures in monolayer TMDs, which are trigonal prismatic (1H) and octahedral (1T) coordination, respectively [26]. For the 1H structure, the chalcogens are vertically aligned along the z-axis and the transition metals are sandwiched in the middle plane along the x-axis, forming Bernal (ABA) stacking (Fig. 1a). When considering the staking periodic of each 1H layer, two and three 1H layers can form the hexagonal 2H and rhombohedral 3R structures, respectively [2, 3]. In contrast, the 1T phase has octahedral coordination with the tetragonal symmetry in which three atomic planes have a rhombohedral

Fig. 1 Atomic structures and ground-state energy of monolayer transition metal dichalcogenides MX_2 (M = W, Mo; X = Te, Se and S). **a** 1H-MX_2 in ABA stacking with the $P\bar{6}m2$ space group; **b** 1T-MX_2 in ABC stacking with the $P\bar{3}m2$ space group; **c** The atomic structure of 1T'-MX_2 (distorted 1T-MX_2), where the distorted M atoms form 1D zigzag chains indicated by the dashed blue line. The unit cell is indicated by red rectangles. **a–c** Reproduced with permission from Ref. [26] Copyright 2014, American Association for the Advancement of Science (AAAS); **d** Ground-state energy differences between monolayer phases of the MX_2. The energy U is given per formula unit MX_2 for the 2H, 1T and 1T' phases. Reproduced with permission from Ref. [43] Copyright 2014, Nature Publishing Group

(ABC) stacking (Fig. 1b). The theoretical investigation suggests that the 1T phase is metastable in the free-standing situation, which spontaneously degenerates into monoclinic 1T' [20] (Fig. 1c) and/or orthorhombic T_d crystal structures [8, 22]. In group VI TMDs, the H phase is typically thermodynamically stable and well studied [13, 27–32]. However, it should be noticed that there is an exception, WTe_2, whose T_d phase is stable under an ambient condition [7, 23, 33].

Monolayer TMDs exhibit unique electrical properties, including semiconducting, semi-metallic, metallic and superconducting properties, which strongly depend on the d orbital electron density of the transition metals. Taking MoS_2 as an example, the H phase is semiconducting while the T phase is metallic [34]. Moreover, the metastable T structure shows a better performance in applications involving the electronics and hydrogen evolution reaction (HER) when comparing with the typical H phase [9, 34–42]. These polymorph structures of Group VI TMDs have different phase energies, which are clearly revealed by the density functional theory (DFT)-based calculation as shown in Fig. 1d [43]. Based on those data, except for WTe_2, whose 1T' phases exist under an ambient condition, the relaxation energy from 1T to 1T' structure can reach up to several hundreds of meV per formula unit. Therefore, reliable strategies must be designed to conquer the energy gaps to achieve the controlled phase transition, especially in a large scale and high throughput.

In this review, the state-of-the-art investigations of methods to realize the phase transition in Group VI TMDs are briefly summarized (Fig. 2). The methods, including the intercalation by alkaline ions, chemical doping with foreign atoms or electronics, tension and stress engineering, defect triggering and electric-field treatment, are discussed in detail and illustrated by some examples. Finally, we make a conclusion with personal insights and highlight the challenges and opportunities in this field.

2 Ion intercalation

TMDs are van der Waals inorganic solids with weak interlayer cohesion but strong in-plane bonding. Specific elements (e.g., Li, Na, K, P) could intercalate into the crystals, forming a sandwich-like ternary compounds which are highly anisotropic [9–14, 34–42]. The experimentally observed phase transition dates back to as early as 1980s. In that pioneering work, Py and coworkers [10, 15, 44] suggested that electrons from alkali ions could transfer to MoS_2 during the intercalation process, forming an electron density-increased state in the d orbital of the transition metal, thus promoting the instability of the 2H phase and impelling its transition to 1T or 1T' phase (Fig. 3a). Recent theoretical calculations on the lithium-intercalated MoS_2 shows that the stability of phases (e.g., 2H, 1T, 1T') has highly significant correlation with the Li concentration that inserted into MoS_2 crystals [20]. The phase transition from 2H to 1T can be triggered when the intercalated Li (or electron charging) concentration is higher than 20% (or 8.33×10^{14} cm^{-2}). At 100% of the intercalation, the phase of MoS_2 stabilizes at a distorted octahedron-coordinated structure with Mo-Mo clustering due to the excess charges on the expanded monolayers. This charge injection theory can well match the experience and provide a better understanding on crystal structures of monolayer TMDs. However, the specific

Fig. 2 Schematic diagram of the phase transition strategies of Group VI TMDs (M = W, Mo; X = Te, Se and S). V1 stands for the vacancy of M, V2 stands for the vacancy of X. A stands for intercalated ions such as alkali metal reagents, ammonia-ions and light-weight nonmetal elements. Black arrows indicate the sliding directions of M and/or X. M′ and X′ stands for heteroatoms, which have different atomic number as M and X, respectively
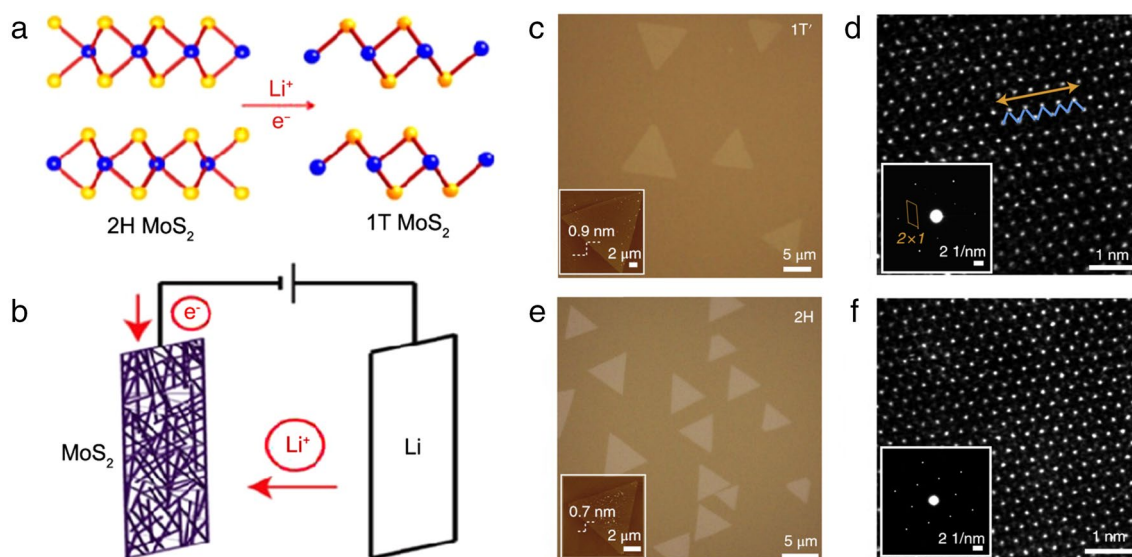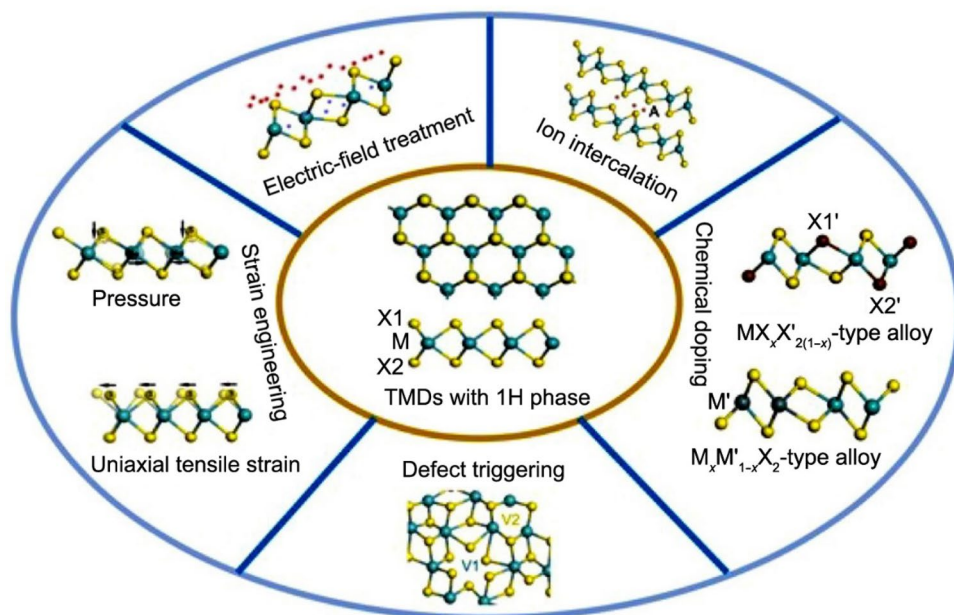
Fig. 3 Schematic illustration of the phase transition from 2H to 1T (1T′) by the ion intercalation or ion-assisted method. **a** Schematic diagram of the first-order phase transition of the 2H to 1T MoS_2 after Li chemical intercalation. Reproduced with permission [47]. Copyright 2014, American Chemical Society (ACS); **b** Schematic representation of the pouch battery cell configuration for Li electrochemical intercalation into MoS_2. Reproduced with permission [40]. Copyright 2014, ACS; **c**, **e** Optical images of 1T′ and 2H mon-olayer MoS_2 flakes grown on mica, respectively. Insets of **c**, **e**: atomic force microscopy (AFM) images of 1T′ and 2H monolayer MoS_2, respectively; **d**, **f** Atomically resolved filtered scanning transmission electron microscopy (STEM) images of 1T′ and 2H MoS_2 flakes, respectively. Insets of **d**, **f**: selected area electron diffraction (SAED) patterns of 1T′ and 2H MoS_2 flakes, respectively. **c–f** Reproduced with permission [51]. Copyright 2018, Nature Publishing Group

evolution of intermediate phases between stable 2H and metastable 1T structures, as well as the atomic mechanisms of how and where the phase transition occurs within the 2H structure are still unclear [25]. Thus, more efforts are needed to elucidate the phase transition processes, especially in the atomic scale.

Typically, alkali metal reagents [9, 10, 12, 15, 16, 41, 44–52], ammonia-ions [53] and light-weight nonmetal elements [42, 54] possess the ability to occupy the inter-space between TMD layers, affording the exfoliation and in-plane phase transition. The most frequently used reagent in traditional chemical intercalation is the hexane solution

of n-Butyllithium when pursuing the phase engineering of Group VI TMDs. For example, Goki Eda and coworkers [55] isolated MoS_2 via Li intercalation, and detected the phase structures of 2H, 1T and 1T′ using high-resolution STEM. Similarly, WS_2 nanosheets with the 1T′ phase can be achieved using chemical exfoliation, in which the W-W chains show a zigzag-like local lattice [38]. Another example was made by Zheng and coworkers [56], and they developed a two-step expansion and intercalation method, where hydrazine (N_2H_4) was used for a series of TMDs pre-exfoliation, followed with the intercalation by aphthalenide adducts ($A^+C_{10}H_8^-$, A = Li, Na, K). Most of the obtained TMD nanosheets were determined to be single-layered and exhibited both 1H and 1T structures. Moreover, the layer-dependent phase transition behavior of TMDs was revealed by Sun and coworkers [57]. Assisted with the STEM and back-gated field-efect transistor (FET) measurement, it was found that the duration required for the phase transition decreased with the increasing number of layers. DFT calculation suggests that the Femi level position and phase transition energy of monolayer MoS_2 are higher than those of few layers MoS_2. In other words, more critical-injected electron concentrations are required for one-layer TMDs compared to those with thicker ones [57], which is highly consistent with the experimental tendencies. Based on the solution chemical intercalation, reagents other than alkali metal ions such as ammonia-ions can also be used for pursuing the phase engineering. As an alternative method, Liu and coworkers [53] obtained ammonia-ion-intercalated 1T WS_2 nanoribbons with the high stability via a hydrothermal synthetic strategy.

All the aforementioned chemical intercalation processes were achieved in various solutions, but recently, the solvent-free method is developed in which the raw materials of intercalated reagents and TMDs (or TMD precursors) are mixed together directly and maintained in a solid state. Previous study suggests that the lithiation of MoS_2 can be achieved by annealing the mixture of lithium borohydride ($LiBH_4$) and MoS_2 powders at 300 °C [35]. The concentration of 1T MoS_2 nanosheets reaches ~ 80%. What's more, a liquid-ammonia-assisted lithiation route was developed by Yin and coworkers [36] for achieving the exfoliation and phase engineering of TMDs. In this strategy, bulk MoS_2 powders and lithium pieces were mixed in a tube first, and then high-purity ammonia gas was introduced and condensed into liquid when pursuing the phase transition reaction. The crystal signatures can be imaged by Raman spectra, X-ray diffraction(XRD) spectra, and electron spin resonance(ESR) spectra. Due to the highly diffusive property, lithium vapor was introduced to facilitate the intercalation and phase transition of MoS_2. For example, Tan and coworkers [58, 59] using evaporated lithium atoms to intercalate TMD crystals, achieving the 2H-to-1T′ phase conversion with various ratios by controlling the lithium vapor concentration under

an ultrahigh vacuum situation. Furthermore, light-weight nonmetal elements such as P can be directly used to induce the phase transition of TMDs [42, 54]. Red phosphorus vapor was introduced to react with commercial bulk 2H phase MoS_2 under the protection of an argon (Ar) atmosphere, achieving the intercalation and partial in-plane phase conversion of MoS_2 [42]. This simple one-pot synthesis strategy has potential to produce various TMDs with hybrid structures and flourishes the method of solvent-free phase engineering.

Electrochemical lithium intercalation, different from the typically chemical intercalation methods as mentioned above, is developed to achieve the controlled phase transition and high-yield exfoliation of Group VI TMDs [39, 40, 60, 61]. Generally, the electrochemical lithiation process was achieved in a battery test system as schematically shown in Fig. 3b, where the anode and cathode are lithium foil and various TMDs, respectively. The intercalated lithium concentration can be monitored by precise controlling the current and cut-off voltage during the galvanostatic discharge process [39, 60]. Assisted with liquid exfoliation, high-quality monolayer TMDs with metastable phases can be prepared. This strategy provides an effective approach to finely control the phase refactoring process.

Chemical intercalation is an effective way to induce the phase engineering, but it belongs to post-growth strategies. As an alternative method, the direct synthesis of large-scale 1T(1T′)-TMDs via a simple one-pot-like preparation process is meaningful not only for fundamental researches, but also for practical applications. Inspired by this, Yu and coworkers [9] developed a facile and robust method for the synthesis of micrometer-sized 1T′-MoX_2 (X = S, Se) crystals by annealing and post-treatment of the mixture of S and K_2MoO_4 powders. The obtained samples had a high-purity 1T′ phase and showed a good stability during the HER test, which might be attributed to the electron density changes of Mo by the presence of potassium. Similarly, Liu et al. [51] recently used K_2MoO_4 and S powders as precursors, achieving the high throughput synthesis of 1T′-MoS_2, 2H-MoS_2, and 1T′/2H-heterophase-MoS_2, respectively, by accurate tuning of the reaction atmosphere during the chemical vapor deposition (CVD) process. The high-purity 1T′ and 2H monolayer MoS_2 flakes were verified by optical microscopy (OM), AFM and STEM analyses (Fig. 3c–f). More importantly, the obtained 1T′ phase MoS_2 monolayers showed a long-time air stability. DFT calculations suggest that the K^+ concentration in the CVD-grown MoS_2 is a decisive factor, as there is a threshold to reverse the stability of 1T′- and 2H-MoS_2. The 1T′ phase becomes more stable than the 2H phase when the potassium absorption exceeds 44% [51]. Interestingly, the combination of alkali metal halides (such as NaCl, KBr and KI) and catalytic metal oxides (such as Fe_3O_4, In_2O_3, NiO and Cr_2O_3) is critical to facilitate the

growth of 1T WS$_2$ in a low-pressure CVD system. Lin and coworkers [31] found that iron oxides or indium oxide promoted the formation of butterfly-like grain boundaries rather than the typical triangular types. The growth was found to undergo dramatical suppression when the metal oxides were present. Meanwhile, they indicated that the WS$_2$ butterfly consisted of two symmetrical wings with one side in the 1T phase and the other in the 2H phase. The resulted 1T/2H WS$_2$ heterostructure forms a natural metal-semiconductor junction and can have great potential in applications like ultrathin 2D Schottky diodes and more complicated logic circuits. This direct synthesis strategy has a bright prospect, but its investigation is still in the infancy. That is to say, very limited Group VI TMDs can achieve the phase transition by this method. It is necessary to do more efforts to extend the direct-growth-strategy to other 2D materials beyond Group VI TMDs.

3 Chemical doping

Compared with the ion intercalation-induced phase transition, doping with other elements can precisely process Group VI TMDs with alternating 1T (1T′, T_d) and 1H crystal structures. Generally, the concentration of substituted atoms in alloyed TMDs can be at an arbitrary proportion. The theoretical investigation suggests that the formation of ternary alloys should meet three rules: (1) $|\alpha_1 - \alpha_2|/\max(\alpha_1, \alpha_2) < 0.034$, (2) $\Delta d_{M-X} < 0.01$ nm, and (3) $(E_{g1} > 0)$ V $(E_{g2} > 0)$, respectively, where α_1 and α_2 are the lattice constants of the two TMD materials, Δd_{M-X} is the difference in the metal-chalcogen bond distance, and E_{g1} and E_{g2} are their band gaps [62]. Rule (1) reflects that the lattice constants must be well matched, which means that the mismatch ratio between two atoms should be smaller than 3.4%. Similar to the first one, rule (2) illustrates that the bond distance of transition metal-chalcogen needs to be less than 0.01 nm. And rule (3) requires that at least one of the TMDs compounds is a semiconductor. The driving force for the 2H-to-1T(1T′) phase transition is an electron donation process of transition metal atoms, which destabilized the 2H phase to transform to the 1T (1T′) phase [63]. Ternary TMDs alloys, the most investigated system in phase engineering, can be synthesized by two doping approaches, which include substituting isoelectronic chalcogens or transition metals, resulting in $M_xM'_{1-x}X_2$- or $MX_xX'_{2(1-x)}$-type alloys.

In a $MX_xX'_{2(1-x)}$-type alloy, one of the chalcogens atoms (X) in the Group VIA is partially substituted by another one (X'), achieving the phase transition (exampled by Fig. 4a). Generally, WSe$_2$ is a p-type semiconductor
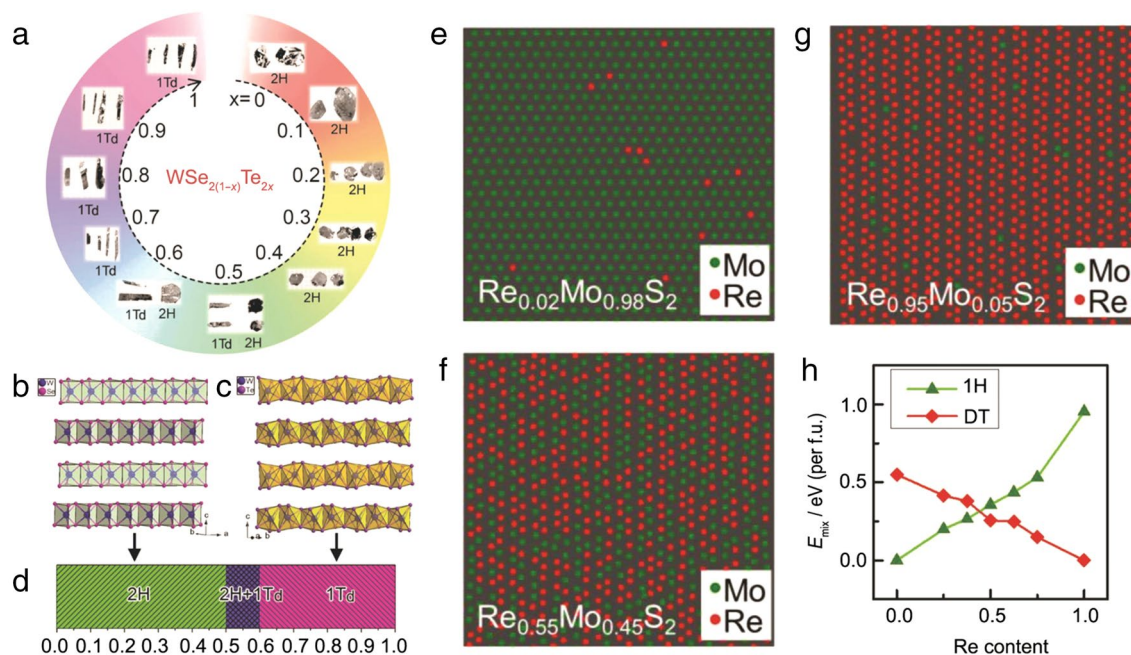
Fig. 4 Chemical doping-induced phase transition. **a** Photographs of as-grown WSe$_{2(1-x)}$Te$_{2x}$ ($x=0$–1) single crystals on the millimeter-grid paper, and 2H and 1T$_d$ types of TMD alloys with circularly platy and bar shapes, which are in agreement with hexagonal and orthorhombic crystal systems, respectively; **b** The crystal structure of 2H WSe$_2$. **c** The crystal structure of 1T$_d$ WTe$_2$; **d** Different phases with dependence of the concentration x in WSe$_{2(1-x)}$Te$_{2x}$. **a–d** Reproduced with permission from Ref. [64] Copyright 2017, John Wiley & Sons, Inc; **e–g** Experimental STEM-annular dark-field (ADF) images with different Re doping concentrations. The Re and Mo atoms are identified by image intensities; **h** Calculated mixing energy in 1H and DT phase Re$_x$Mo$_{1-x}$S$_2$ alloys at different Re concentrations. **e–h** Reproduced with permission from Ref. [67] Copyright 2018, John Wiley & Sons, Inc

with a 2H crystal structure (Fig. 4b), while WTe_2 is a semimetal with the $1T_d$ phase (Fig. 4c), with marriage of the two isolated materials to form a ternary layer, and the semiconductor-metal phase transition can be realized. For instance, Yu and coworkers [64] synthesized the $WSe_{2(1-x)}Te_{2x}$ ($x = 0–1$) alloys using chemical vapor transport (CVT), and systematically investigated the relationship between different phases and the concentration x in $WSe_{2(1-x)}Te_{2x}$ ($x = 0–1$) alloys (Fig. 4a). As shown in Fig. 4a, d, the gradual structure transition from 2H to T_d phases were observed when tuning the concentration x from 0 to 100%: specifically, $x = 0–0.4$ for the 2H structure, $x = 0.5–0.6$ for both 2H and $1T_d$ structures, and $x = 0.7–1.0$ for the $1T_d$ structure. Examined with the STEM images, no intrinsic defects such as grain boundaries and dislocations were observed, suggesting that the phase transition might occur at the very beginning growth of the ternary alloy [64].
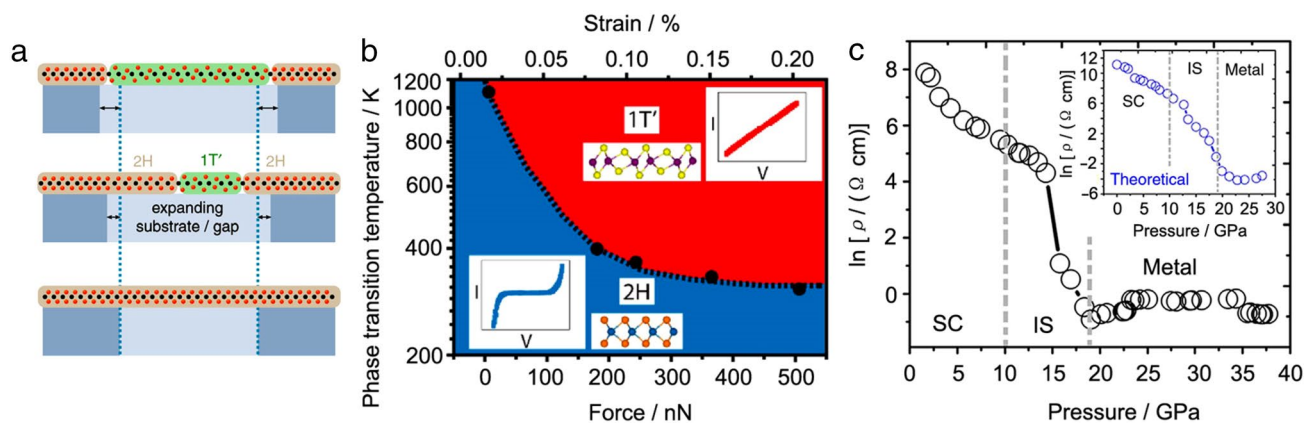
As for $M_xM'_{1-x}X_2$-type alloys, the transition metal elements (M) in TMDs replaced by atoms with different atomic numbers can induce the crystal structure transition. Experimental and theoretical investigation suggests that $MoTe_2$ and WTe_2 have the akin crystal structures. However, the stable phases of these two materials at room temperature are 2H (or 1T′) and T_d, respectively. Phase engineering can be achieved by alloying the host materials. For example, Rhodes and coworkers [65] engineered the crystal structures of $MoTe_2$ through W substitution, achieving the phase transition from semiconducting 2H-phase to semimetal T_d phase. It is clearly seen that the orthorhombic T_d phase is thermodynamically preferred over the hexagonal 2H-phase when the concentration of W is higher than 0.08. Similarly, MoS_2 is also an ideal host material to investigate the structure conversation due to its ample nature in phases. For example, Yang and coworkers [66] reported a facile one-pot liquid-phase synthesis of $Mo_{1-x}W_xS_2$ alloy with tunable 1T/2H phase concentrations, in which the ratios could be modulated by varying the reaction temperature. Apart from doping with elements from the same group, atoms from other groups can also be used when pursuing the phase engineering. Kochat and coworkers [63] developed a CVD process to synthesize the Re-doped $MoSe_2$ and found that the 1T′ phase could be stabilized by increasing the Re concentration in the host material. DFT calculations suggest that the extra electron is promoted to a higher energy level and destabilizes the 2H phase, which means that the stability of 1T (1T′) phase increased. Similarly, Yang and coworkers [67] prepared a series of highly stable distorted tetragonal (DT) $Re_xMo_{1-x}S_2$ alloys in a CVD system and investigated the phase structures via STEM. As shown in Fig. 4e, the MoS_2 could be stable at the 1H phase with a small amount of Re (2–4%). The DT phase was found when the Re concentration was beyond 50% (Fig. 4f, g), which was in agreement with calculated

results as shown in Fig. 4h. They also suggested that the crystal structure transition from 1H- to DT-phase could be well explained by the crystal field theory.

4 Strain engineering

The tensile or compressive strain loading on TMDs crystals can lead to a relative sliding of atomic positions, forming a modified structure with interesting chemical [37] and physical [43, 68–72] properties. Different from the aforementioned chemical modification methods, generally, strain engineering is a physical regulation process. Previous theoretical investigations indicated that most of the Group VI TMDs could acquire metallic phases under the equibiaxial tensile strains of 10%–15% due to the overlapping of d_{z^2} orbital at the Fermi level [43, 68]. Considering the loading mode of stain, the biaxial tensile strain, uniaxial tensile strain, and pure shear strain can reduce the band gap of TMDs in varying levels, respectively [68]. In particular, the phase transition is extremely sensitive to the biaxial tensile strain compared to the uniaxial tensile strain. Taking the variety of chalcogenides as consideration, the band gap of monolayer MSe_2 and MTe_2 decrease faster than that of MS_2 when the pure shear strain is applied [68]. Tensile strain also has the ability to switch thermodynamic stability between stable 2H and metastable 1T (1T′) phases (Fig. 5a). For example, Duerloo and coworkers [43] systematically introduced the relationships between phase diagrams of Group VI TMDs and tensile strain using DFT-based simulations. Depending on their calculations, the strain needed for phase conversion of $MoTe_2$ is as low as 0.3%–3% at room temperature. This indicates that the $MoTe_2$ is an excellent candidate material for the investigation of the crystal structure modification.

A great number of first principle calculations are reported as mentioned above, paving the way for the realization of the phase transition of Group VI TMDs in a theoretical perspective. The experimental introduction of strains in TMDs can be achieved by three methods, including bending the flexible substrates where the sample loaded on, and applying pressure using the AFM tip or high-pressure diamond anvil cell (DAC), leading to the lattice distortion and thus forming the phase transition. A recent report from He and coworkers [69] demonstrated the continuous modification of the electronic signature of MoS_2 layers on a flexible supporting substrate by loading an uniaxial tensile strain. Using optical absorption and photoluminescence (PL) spectroscopy, they found that the exciton redshift at a rate of ~70 meV/% strain for monolayer MoS_2, and a larger rate (1.6 times higher) for bilayer MoS_2 under a relatively small strain. Moreover, Manzeli and coworkers [72] established the connection between the strain-induced bandgap changes

and electrical performance of MoS$_2$, suggesting that the bandgap decreased with the tensile strain augmentation. Different from the bending-induced strains mentioned above, strains were applied using an AFM tip. Similarly, Song and coworkers [73] investigated the phase transition temperature of MoTe$_2$ by introducing a tensile strain via an AFM tip. As shown in Fig. 5b, the first-order phase transition temperature of 2H MoTe$_2$ gradually decreases when increasing the strain levels. Especially, the semiconductor-metal (S-M) transition can be accomplished at room temperature under a small tensile strain of 0.2%. The crystal structure transition was identified by current atomic force microscopy (CAFM). Interestingly, the observed S-M phase transition is fully reversible under the ambient condition after the release of strains. Recently, Nayak and coworkers [70] revealed the optical, structural, electrical and vibrational nature of few-layer MoS$_2$ under various pressure conditions in a DAC device. Pressure-induced phase structure can be divided into three categories including semiconducting (SC) at 0–10 Gpa, intermediate state (IS) at 10–19 Gpa, and metallic regions beyond 19 Gpa (Fig. 5c). Theoretical calculation suggested that high pressure would decrease the conduction band minima from S-p$_x$ and S-p$_y$ orbitals, and increase the valence band maximum from S-p$_z$ orbitals, forming an overlap state.

5 Defect triggering

Structural defects in TMDs, including grain boundaries, point defects and edges, have a significant impact on the electrical, optical, mechanical, and chemical properties of the material. Due to the atomic thin dimensions, mono- or few-layer TMDs are greatly sensitive to the presence of defects, especially to metal or chalcogen vacancies, which can induce the phase transitions [71, 73–78]. Previous studies on MoS$_2$ suggested that S-vacancies and Mo-vacancies might induce the n-type and p-type doping, respectively [74]. In another classic work reported by Zhou and coworkers [77], they developed a facile and robust strategy for the synthesis of high-quality large-area few-layer 2H and 1T′ MoTe$_2$ (Fig. 6a). The MoTe$_2$ with different phases can be achieved by tuning the supply efficiency of Te when reacting with MoO$_3$. For an insufficient Te supply, 1T′ MoTe$_2$ preferred to form due to more vacancies of Te, while 2H MoTe$_2$ were obtained under a Te sufficient environment. The similar conclusions were also reported by Keum and coworkers [75]. They found that, under an excess Te content situation, the 1T′ MoTe$_2$ was transformed to the 2H phase under a slow cooling rate and a new mixed phase was formed in the temperature ranging between 500 °C and 820 °C (Fig. 6b).

Different from the direct control of vacancies during the synthesis process, post-growth defect triggering will be more valuable for engineering the crystal structure. In this regard, the phase transition in TMDs can be induced by irradiation of the high energy source, including laser [76], Ar plasma [78], and electron beam [79]. For example, Cho and coworkers [76] realized the phase transition of MoTe$_2$ from the 2H to the 1T' phase via laser irradiation. Low-density Te vacancies were created on the 2H MoTe$_2$ nanosheet during the laser irradiation. When the concentration of Te monovacancy exceeds 3%, the lattice symmetry of the 2H structure will be broken, forming the 1T' phase (Fig. 6c). Another example was introduced by Zhu and coworkers [78], they suggested that the weak Ar plasma treatment could induce S-vacancies in monolayer MoS$_2$ to active the 2H to 1T phase transition (Fig. 6d). It is
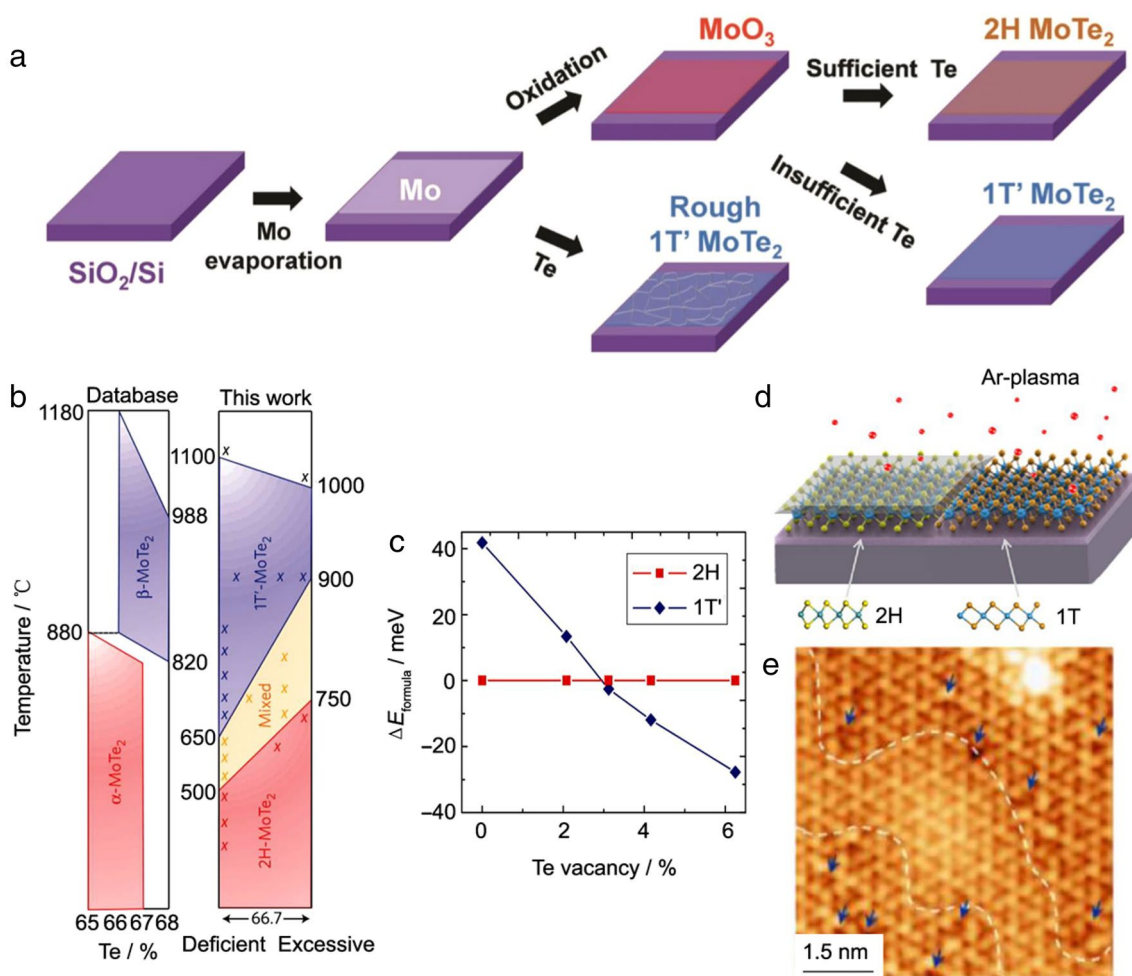
Fig. 6 Defects-induced phase transition. **a** Schematic illustration of the growth process for 1T′ and 2H MoTe$_2$ using Mo and MoO$_3$ as precursors. Reproduced with permission from Ref. [77] Copyright 2016, John Wiley & Sons, Inc; **b** Alloy phase diagram of MoTe$_2$ in the ASM database (left) and the new phase diagram based on experimental work (right). Reproduced with permission from Ref. [75] Copyright 2015, Nature Publishing Group; **c** Energy differences between 2H and 1T′ phases as a function of the Te vacancy concentration from the DFT calculation. Reproduced with permission from Ref. [76] Copyright 2015, AAAS; **d** Schematic representation of the plasma-treated process; **e** High-resolution STM images of monolayer MoS$_2$ on graphite after the 40-s phase transition treatment. The S vacancies were highlighted by blue arrows. **d–e** Reproduced with permission from Ref. [78] Copyright 2017, ACS

clear that the sliding of the top S layer is kinetically spontaneous under Ar plasma irradiation. After 40-s treatments, the concentration of the 1T phase can be up to 40%, and the S vacancies can be clearly observed in high-resolution scanning tunneling microscopy (STM) image (Fig. 6e). Recently, Lin and coworkers [79] investigated the phase transition of slightly Re-doped MoS$_2$ via an electron beam irradiation strategy, suggesting that the phase conversation was driven by the gliding of the atomic planes of S and/or Mo. The semiconducting to metallic phase transition begins at the intermediate phase (α-phase), and the migration of two kinds of boundaries (β- and γ-boundaries) was responsible for the growth of the second phase.

6 Electric-field treatment

Despite the aforementioned attempts to realize a semiconductor-to-metal (S-M) phase transition, it still remains challenging on achieving a reversible structure conversation between 1H and 1T phase in the limit of a monolayer. Previous investigations based on DFT calculations suggested that a reversible S-M phase transition in
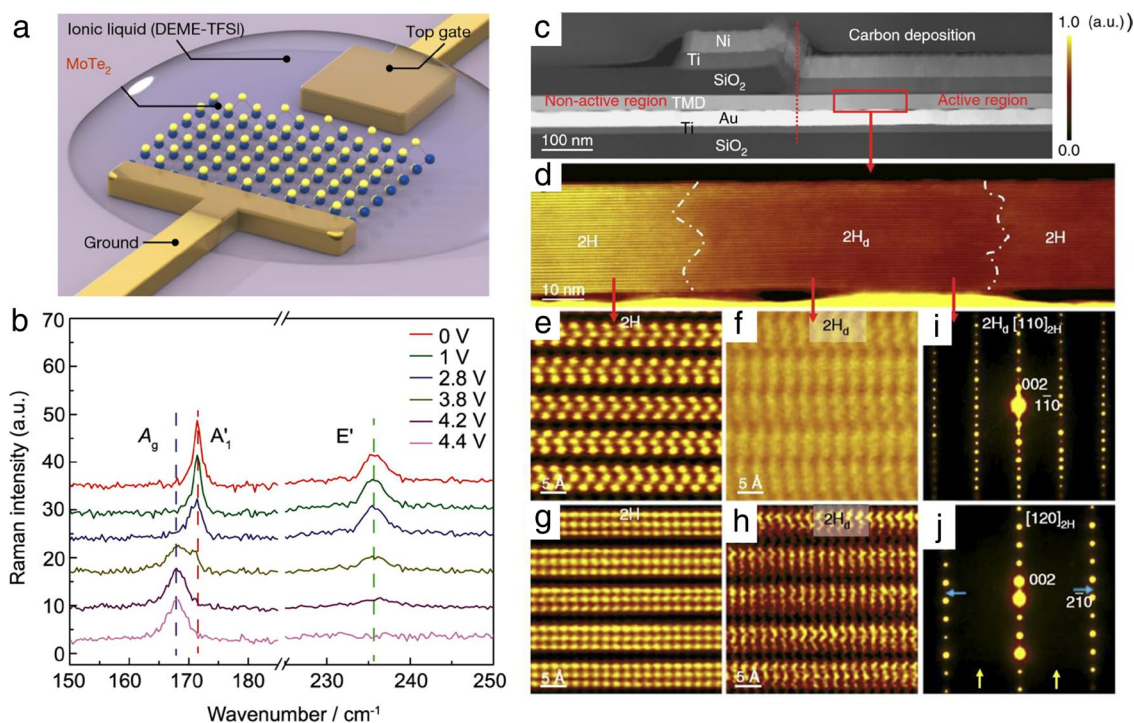
Fig. 7 Electric-field-induced phase transition. **a** Schematic configuration of a monolayer $MoTe_2$ FET; **b** Representative Raman spectra before, during and after transition from the 2H to 1T′ phase, as the bias changes from 0 to 4.4 V. **a–b** Reproduced with permission [82]. Copyright 2017, Nature Publishing Group; **c** HAADF-STEM image of the cross-section of the $Mo_{0.96}W_{0.04}Te_2$ device; **d** Higher magnification of the HAADF image from the region defined by a red box in **c** and showing the coexistence of a distorted structure ($2H_d$) with 2H; **e–h** Atomic-resolution HAADF images along **e**, **f** the $[110]_{2H}$ zone axis and **g**, **h** $[120]_{2H}$ zone axis, showing the intact 2H and distorted $2H_d$ structures, respectively; **i**, **j** Corresponding nanobeam diffraction pattern from the distorted $2H_d$ area, which was still indexed as the 2H structure. False colors were added. **c–j** Reproduced with permission from Ref. [83] Copyright 2019, Nature Publishing Group

some single-layer TMDs, including $MoTe_2$, $Mo_xW_{1-x}Se_2$, MoS_2, and $TaSe_2$, could be realized by applying electrostatic gating [80, 81]. The carrier density and electron chemical potential for a monolayer TMD could be changed under various gate voltages, inducing the phase transition from semiconducting to metallic. They also calculated the surface charge density (SCD) required for the phase transition: for monolayer $MoTe_2$ under a constant stress condition, the SCD could be less than -0.04 e or greater than 0.09 e per formula unit; while for monolayer MoS_2, the values become -0.29 e and 0.35 e per formula unit, respectively [80].

Wang and coworkers [82] experimentally realized the electrostatic-doping-driven phase conversation, introducing the ionic liquid FET (Fig. 7a) to reveal the relationship between the phase structures and gate voltages. Assisted by Raman spectroscopy, it was reported that the 1T' phase was gradually formed under the gate control, illustrating that the 2H phase would completely transform to 1T' phase at the bias of 4.4 V (Fig. 7b). Interestingly, a reversible phase conversation was achieved by increasing or decreasing the bias voltage. Essentially, the structural phase transition could be driven by the ground-state switching of 2H or 1T' phase,

as extra electrons from electrostatic doping were expected to lift the total energy of the 2H phase above that of the 1T′ phase, resulting in the metastable 2H phase. Another inspiring work elucidated an electric-field-induced structure conversation from a 2H to a $2H_d$ and T_d phase in a vertical $2H$-$MoTe_2$- and $Mo_xW_{1-x}Te_2$-based resistive random access memory (RRAM) device [83]. Using STEM can sufficiently reveal the $2H_d$ crystal structure, which is formed after a set voltage application (Fig. 7c–j). The $2H_d$ phase is a transient state with a semiconducting to metallic behavior, which can drop back to the high resistive state at the temperature of 523 K according to temperature-dependent electrical measurement. However, the driving force for the formation and stabilization of the $2H_d$ phase is still unclear.

7 Conclusion

In summary, the recent progress in the phase-controlled synthesis or post-growth engineering of Group VI TMDs is discussed. Phase engineering in Group VI TMDs can be realized using alkaline ions intercalation, doping with foreign atoms or electronics, applying tension and stress,

defect triggering, electron injection and other feasible strategies. Intercalation by alkaline metal has a long history and is widely investigated due to its reproducible and feasible nature when pursuing the phase modification. As typical post-growth strategies, the strain and defect treatments can efficiently engineer the optical, electrical and structural properties of Group VI TMDs, which have potential applications in photoelectronic, low-connect-resistance and energy-harvesting devices. Doping with heteroatoms is another efficient way to switch the ground state of basic materials. The recent results on the electrostatic-doping-driven phase transition of two-dimensional layered materials show potential applications in memory and reconfigurable devices. Meanwhile, metallic phases provide a versatile platform for investigations on the fundamental physical and chemical phenomenon.

Despite the great progress already made in this research field, some challenges still remain to be solved. As mentioned above, most of the metallic structure of Group VI TMDs is metastable, so that spontaneous reverting back to the semiconducting state due to the thermodynamic instability need to be settled. Several compromised methods, including surface functionalization and intercalated Li hydrogenation, have been developed for enhancing the stability of metallic TMDs. However, the surface-doping strategies could degenerate the surface functional properties, while Li hydrogenation usually asks for an ultrahigh vacuum condition. Aforementioned methods significantly sacrifice the extensibility of metallic phase TMDs. Another challenge is the controllability to realize the metal-insulator transition, especially at an ambient condition. Clearly, post-growth conversion strategies are typical methods to achieve the phase conversion, but its operation process is complicated. Thus, developing a direct phase-controlled synthesis route is necessary. CVD is one of the most promising alternative methods for the controllable synthesis of layered materials, which can be used in phase engineering. But its investigation is still in the infancy. Thus, more efforts are still necessary to get the controllable phase transition in Group VI TMDs and a stable phase transition is necessary for their real applications.

References

1. Voiry D, Mohite AD, Chhowalla M. Phase engineering of transition metal dichalcogenides. Chem Soc Rev. 2015;44(9):2702.
2. Manzeli S, Ovchinnikov D, Pasquier D, Yazyev OV, Kis A. 2D transition metal dichalcogenides. Nat Rev Mater. 2017;2(8):17033.
3. Wang JL, Wei Y, Li H, Huang X, Zhang H. Crystal phase control in two-dimensional materials. Sci China Chem. 2018;61(10):1227.
4. Ma Y, Ajayan PM, Yang SB, Gong YJ. Recent advances in synthesis and applications of 2D junctions. Small. 2018;14(38):1801606
5. Fiori G, Bonaccorso F, Iannaccone G, Palacios T, Neumaier D, Seabaugh A, Banerjee SK, Colombo L. Electronics based on two-dimensional materials. Nat Nanotech. 2014;9(10):768.
6. Huang LN, McCormick TM, Ochi M, Zhao ZY, Suzuki MT, Arita R, Wu Y, Mou DX, Cao HB, Yan JQ, Trivedi N, Kaminski A. Spectroscopic evidence for a type II Weyl semimetallic state in MoTe$_2$. Nat Mater. 2016;15(11):1155.
7. Tang SJ, Zhang CF, Wong D, Pedramrazi Z, Tsai HZ, Jia CJ, Moritz B, Claassen M, Ryu H, Kahn S, Jiang J, Yan H, Hashimoto M, Lu DH, Moore RG, Hwang CC, Hwang CY, Hussain Z, Chen YL, Ugeda MM, Liu Z, Xie XM, Devereaux TP, Crommie MF, Mo SK, Shen ZX. Quantum spin Hall state in monolayer 1T'-WTe$_2$. Nat Phys. 2017;13(7):683.
8. Wu Y, Mou DX, Jo NH, Sun KW, Huang LN, Bud'ko SL, Canfield PC, Kaminski A. Observation of Fermi arcs in the type-II Weyl semimetal candidate WTe$_2$. Phys Rev B. 2016;94(12):121113.
9. Yu YF, Nam GH, He QY, Wu XJ, Zhang K, Yang ZZ, Chen JZ, Ma QL, Zhao MT, Liu ZQ, Ran FR, WangXZ Li H, Huang X, Li B, Xiong QH, Zhang Q, Liu Z, Gu L, Du YH, Huang W, Zhang H. High phase-purity 1T'-MoS$_2$- and 1T'-MoSe$_2$-layered crystals. Nat Chem. 2018;10(6):638.
10. Wilson JA, Yoffe AD. The transition metal dichalcogenides discussion and interpretation of the observed optical, electrical and structural properties. Adv Phys. 1969;18(73):193
11. Jiménez Sandoval S, Yang D, Frindt RF, Irwin JC. Raman study and lattice dynamics of single molecular layers of MoS$_2$. Phys Rev B. 1991;44(8):3955.
12. Yang D, Sandoval SJ, Divigalpitiya WMR, Irwin JC, Frindt RF. Structure of single-molecular-layer MoS$_2$. Phys Rev B. 1991;43(14):12053.
13. Radisavljevic B, Radenovic A, Brivio J, Giacometti V, Kis A. Single-layer MoS$_2$ transistors. Nat Nanotech. 2011;6(3):147.
14. Mak KF, Lee C, Hone J, Shan J, Heinz TF. Atomically thin MoS$_2$: a new direct-gap semiconductor. Phys Rev Lett. 2010;105(13):136805
15. Martin BD. Lithium intercalation via n-Butyllithium of the layered transition metal dichalcogenides. Mat Res Bull. 1975;10(4):287.
16. Chrissafis K, Stoemenos J, Economou NA. Structural studies of MoS$_2$ intercalated by lithium. Mat Sci Eng B. 1989;3(1):145.
17. Rocquefelte X, Boucher F, Gressier P. Mo cluster formation in the intercalation compound LiMoS$_2$. Phys Rev B. 2000;62(4):2397.
18. Naylor CH, Parkin WM, Ping JL, Gao ZL, Zhou YR, Kim YK, Streller F, Carpick RW, Rappe AM, Drndic M, Kikkawa JM, Johnson AT. Monolayer single-crystal 1T'-MoTe$_2$ grown by chemical vapor deposition exhibits weak antilocalization effect. Nano Lett. 2016;16(7):4297.
19. Calandra M. Chemically exfoliated single-layer MoS$_2$: stability, lattice dynamics, and catalytic adsorption from first principles. Phys Rev B. 2013;88(24):4269
20. Kan M, Wang JY, Li XW, Zhang SH, Li YW, Kawazoe Y, Sun Q, Jena P. Structures and phase transition of a MoS$_2$ monolayer. J Phys Chem C. 2014;118(3):1515.
21. Gao GP, Jiao Y, Ma FX, Jiao YL, Waclawik E, Du AJ. Charge mediated semiconducting-to-metallic phase transition in molybdenum disulfide monolayer and hydrogen evolution reaction in new 1T' phase. J Phys Chem C. 2015;119(23):13124.
22. Sun Y, Wu SC, Ali MN, Felser C, Yan BH. Prediction of Weyl semimetal in orthorhombic MoTe$_2$. Phys Rev B. 2015;92(16):161107.
23. Ma XL, Guo PJ, Yi CJ, Yu QH, Zhang AM, Ji JT, Tian Y, Jin F, Wang YY, Liu K, Xia TL, Shi YG, Zhang QM. Raman scattering

in the transition-metal dichalcogenides of 1T'-MoTe$_2$, T_d-MoTe$_2$, and T_d-WTe$_2$. Phys Rev B. 2016;94(21):214105.

24. Chen ZH, Wang LW. Material genome explorations and new phases of two-dimensional MoS$_2$, WS$_2$, and ReS$_2$ monolayers. Chem Mater. 2018;30(18):6242.

25. Jin Q, Liu N, Chen BH, Mei D. Mechanisms of semiconducting 2H to metallic 1T phase transition in two-dimensional MoS$_2$ nanosheets. J Phys Chem C. 2018;122(49):28215.

26. Qian XF, Liu JW, Fu L, Li J. Quantum spin hall effect in two-dimensional transition metal dichalcogenides. Science. 2014;346:1344.

27. Splendiani A, Sun L, Zhang YB, Li TS, Kim JW, Chim CY, Galli G, Wang F. Emerging photoluminescence in monolayer MoS$_2$. Nano Lett. 2010;10(4):1271.

28. Eda G, Yamaguchi H, Voiry D, Fujita T, Chen M, Chhowalla M. Photoluminescence from chemically exfoliated MoS$_2$. Nano Lett. 2011;11(12):5111.

29. Castellanos-Gomez A, Poot M, Steele GA, van der Zant HS, Agrait N, Rubio-Bollinger G. Elastic properties of freely suspended MoS$_2$ nanosheets. Adv Mater. 2012;24(6):772.

30. Zeng HL, Dai JF, Yao W, Xiao D, Cui XD. Valley polarization in MoS$_2$ monolayers by optical pumping. Nat Nanotech. 2012;7(8):490.

31. Lin YC, Yeh CH, Lin HC, Siao MD, Liu Z, Nakajima H, Okazaki T, Chou MY, Suenaga K, Chiu PW. Stable 1T tungsten disulfide monolayer and its junctions: growth and atomic structures. ACS Nano. 2018;12(12):12080.

32. Bertolazzi S, Brivio J, Kis A. Stretching and breaking of ultrathin MoS$_2$. ACS Nano. 2011;5(12):9709.

33. Zhou W, Chen JZ, Gao H, Hu T, Ruan SC, Stroppa A, Ren W. Anomalous and polarization-sensitive photoresponse of T_d-WTe$_2$ from visible to infrared light. Adv Mater. 2018;1804629.

34. Liu Q, Fang Q, Chu WS, Wan YY, Li XL, Xu WY, Habib M, Tao S, Zhou Y, Liu DB, Xiang T, Khalil A, Wu XJ, Chhowalla M, Ajayan PM, Song L. Electron-doped 1T-MoS$_2$ via interface engineering for enhanced electrocatalytic hydrogen evolution. Chem Mater. 2017;29(11):4738.

35. Voiry D, Salehi M, Silva R, Fujita T, Chen MW, Asefa T, Shenoy VB, Eda G, Chhowalla M. Conducting MoS$_2$ nanosheets as catalysts for hydrogen evolution reaction. Nano Lett. 2013;13(12):6222.

36. Yin Y, Han JC, Zhang YM, Zhang XH, Xu P, Yuan Q, Samad L, Wang XJ, Wang Y, Zhang ZH, Zhang P, Cao XZ, Song B, Jin S. Contributions of phase, sulfur vacancies, and edges to the hydrogen evolution reaction catalytic activity of porous molybdenum disulfide nanosheets. J Am Chem Soc. 2016;138(25):7965.

37. Lukowski MA, Daniel AS, Meng F, Forticaux A, Li LS, Jin S. Enhanced hydrogen evolution catalysis from chemically exfoliated metallic MoS$_2$ nanosheets. J Am Chem Soc. 2013;135(28):10274.

38. Voiry D, Yamaguchi H, Li JW, Silva R, Alves DCB, Fujita T, Chen MW, Asefa T, Shenoy V, Eda G, Chhowalla M. Enhanced catalytic activity in strained chemically exfoliated WS$_2$ nanosheets for hydrogen evolution. Nat Mater. 2013;12(9):850.

39. Wang HT, Lu ZY, Xu SC, Kong DS, Cha JJ, Zheng GY, Hsu PC, Yan K, Bradshaw D, Prinz FB, Cui Y. Electrochemical tuning of vertically aligned MoS$_2$ nanofilms and its application in improving hydrogen evolution reaction. Proc Natl Acad Sci USA. 2013;110(49):19701.

40. Wang HT, Lu ZY, Kong DH, Sun J, Hymel TM, Cui Y. Electrochemical tuning of MoS$_2$ nanoparticles on three-dimensional substrate for efficient hydrogen evolution. ACS Nano. 2014;8(5):4940.

41. Chang K, Hai X, Pang H, Zhang HB, Shi L, Liu GG, Liu HM, Zhao GX, Li M, Ye J. Targeted synthesis of 2H- and 1T-phase MoS$_2$ monolayers for catalytic hydrogen evolution. Adv Mater. 2016;28(45):10033.

42. Wang S, Zhang D, Li B, Zhang C, Du ZG, Yin HM, Bi XF, Yang SB. Ultrastable in-plane 1T-2H MoS$_2$ heterostructures for enhanced hydrogen evolution reaction. Adv Energy Mater. 2018;8(25):1801345.

43. Duerloo KA, Li Y, Reed EJ. Structural phase transitions in two-dimensional Mo- and W-dichalcogenide monolayers. Nat Commun. 2014;5:4214.

44. Somoano RB, Hadek V, Rembaum A. Alkali metal intercalates of molybdenum disulfide. J Chem Phys. 1973;58(2):697.

45. Cheng YC, Nie AM, Zhang QY, Gan LY, Reza SY, Udo S. Origin of the phase transition in lithiated molybdenum disulfide. ACS Nano. 2014;8(11):11447.

46. Heising J, Kanatzidis MG. Structure of restacked MoS$_2$ and WS$_2$ elucidated by electron crystallography. J Am Chem Soc. 1999;121(4):638.

47. Wang LF, Xu Z, Wang WL, Bai XD. Atomic mechanism of dynamic electrochemical lithiation processes of MoS$_2$ nanosheets. J Am Chem Soc. 2014;136(18):6693.

48. Kappera R, Voiry D, Yalcin SE, Branch B, Gupta G, Mohite AD, Chhowalla M. Phase-engineered low-resistance contacts for ultrathin MoS$_2$ transistors. Nat Mater. 2014;13(12):1128.

49. Guo YS, Sun DZ, Ouyang B, Raja A, Song J, Heinz TF, Brus LE. Probing the dynamics of the metallic-to-semiconducting structural phase transformation in MoS$_2$ crystals. Nano Lett. 2015;15(8):5081.

50. Chen ZX, Leng K, Zhao XX, Malkhandi S, Tang W, Tian BB, Dong L, Zheng LR, Lin M, Yeo BS, Loh KP. Interface confined hydrogen evolution reaction in zero valent metal nanoparticles-intercalated molybdenum disulfide. Nat Commun. 2017;8:14548.

51. Liu LN, Wu JX, Wu LY, Ye M, Liu XZ, Wang Q, Hou SY, Lu PF, Sun LF, Zheng JY, Xing L, Gu L, Jiang XW, Xie LM, Jiao LY. Phase-selective synthesis of 1T' MoS$_2$ monolayers and heterophase bilayers. Nat Mater. 2018;17(12):1108.

52. Wypych F, Schöllhorn R. 1T-MoS$_2$, a new metallic modification of molybdenum disulfide. J Chem Soc, Chem Commun. 1992;19:1386.

53. Liu Q, Li XL, Xiao ZR, Zhou Y, Chen HP, Khalil A, Xiang T, Xu JQ, Chu WS, Wu XJ, Yang JL, Wang CM, Xiong YJ, Jin CH, Ajayan PM, Song L. Stable metallic 1T-WS$_2$ nanoribbons intercalated with ammonia ions: the correlation between structure and electrical/optical properties. Adv Mater. 2015;27(33):4837.

54. Ye LJ, Chen SJ, Li WJ, Pi MY, Wu TL, Zhang DK. Tuning the electrical transport properties of multilayered molybdenum disulfide nanosheets by intercalating phosphorus. J Phys Chem C. 2015;119(17):9560.

55. Eda G, Fujita T, Yamaguchi H, Voiry D, Chen MW, Chhowalla M. Coherent atomic and electronic heterostructures of single-layer MoS$_2$. ACS Nano. 2012;6(8):7311.

56. Zheng J, Zhang H, Dong SH, Liu YP, Tai Nai C, Suk Shin H, Young Jeong H, Liu B, Ping Loh K. High yield exfoliation of two-dimensional chalcogenides using sodium naphthalenide. Nature Commun. 2014;5:2995.

57. Sun LF, Yan XX, Zheng JY, Yu HD, Lu ZX, Gao SP, Liu LN, Pan XQ, Wang D, Wang ZG, Wang P, Jiao LY. Layer-dependent chemically induced phase transition of two-dimensional MoS$_2$. Nano Lett. 2018;18(6):3435.

58. Tan SJ, Abdelwahab I, Ding ZJ, Zhao XX, Yang TS, Loke GZ, Lin H, Verzhbitskiy I, Poh SM, Xu H, Nai CT, Zhou W, Eda G, Jia B, Loh KP. Chemical stabilization of 1T' phase transition metal dichalcogenides with giant optical kerr nonlinearity. J Am Chem Soc. 2017;139(6):2504.

59. Tan SJR, Sarkar S, Zhao XX, Luo X, Luo YZ, Poh SM, Abdelwahab I, Zhou W, Venkatesan T, Chen W, Quek SY, Loh KP. Temperature- and phase-dependent phonon renormalization in 1T'-MoS$_2$. ACS Nano. 2018;12(5):5051.

60. Zeng ZY, Yin ZY, Huang X, Li H, He QY, Lu G, Boey F, Zhang H. Single-layer semiconducting nanosheets: high-yield preparation and device fabrication. Angew Chem Int Ed Engl. 2011;50(47):11289.

61. Zeng ZY, Sun T, Zhu JX, Huang X, Yin ZY, Lu G, Fan ZX, Yan QY, Hng HH, Zhang H. An effective method for the fabrication of few-layer-thick inorganic nanosheets. Angew Chem Int Edit. 2012;51(36):9052.

62. Kutana A, Penev ES, Yakobson BI. Engineering electronic properties of layered transition-metal dichalcogenide compounds through alloying. Nanoscale. 2014;6(11):5820.

63. Kochat V, Apte A, Hachtel JA, Kumazoe H, Krishnamoorthy A, Susarla S, Idrobo JC, Shimojo F, Vashishta P, Kalia R, Nakano A, Tiwary CS, Ajayan PM. Re doping in 2D transition metal dichalcogenides as a new route to tailor structural phases and induced magnetism. Adv Mater. 2017;29(43):1703754.

64. Yu P, Lin JH, Sun LF, Le QL, Yu XC, Gao GH, Hsu CH, Wu D, Chang TR, Zeng QS, Liu FC, Wang QJ, Jeng HT, Lin H, Trampert A, Shen ZX, Suenaga K, Liu Z. Metal-semiconductor phase-transition in WSe$_{2(1-x)}$Te$_{2x}$ monolayer. Adv Mater. 2017;29(4):1603991.

65. Rhodes D, Chenet DA, Janicek BE, Nyby C, Lin Y, Jin W, Edelberg D, Mannebach E, Finney N, Antony A, Schiros T, Klarr T, Mazzoni A, Chin M, Chiu YC, Zheng W, Zhang QR, Ernst F, Dadap JI, Tong X, Ma J, Lou R, Wang S, Qian T, Ding H, Osgood RM Jr, Paley DW, Lindenberg AM, Huang PY, Pasupathy AN, Dubey M, Hone J, Balicas L. Engineering the structural and electronic phases of MoTe$_2$ through W substitution. Nano Lett. 2017;17(3):1616.

66. Yang K, Wang XS, Li H, Chen B, Zhang X, Li SZ, Wang N, Zhang H, Huang X, Huang W. Composition- and phase-controlled synthesis and applications of alloyed phase heterostructures of transition metal disulphides. Nanoscale. 2017;9(16):5102.

67. Yang SZ, Gong YJ, Manchanda P, Zhang YY, Ye GL, Chen SM, Song L, Pantelides ST, Ajayan PM, Chisholm MF, Zhou W. Rhenium-doped and stabilized MoS$_2$ atomic layers with basal-plane catalytic activity. Adv Mater. 2018;30(51):1803477.

68. Johari P, Shenoy VB. Tuning the electronic properties of semiconducting transition metal dichalcogenides by applying mechanical strains. ACS Nano. 2012;6(6):5449.

69. He KL, Poole C, Mak KF, Shan J. Experimental demonstration of continuous electronic structure tuning via strain in atomically thin MoS$_2$. Nano Lett. 2013;13(6):2931.

70. Nayak AP, Bhattacharyya S, Zhu J, Liu J, Wu X, Pandey T, Jin C, Singh AK, Akinwande D, Lin JF. Pressure-induced semiconducting to metallic transition in multilayered molybdenum disulphide. Nat Commun. 2014;5:4731.

71. Zhou L, Xu K, Zubair A, Liao AD, Fang WJ, Ouyang FP, Lee YH, Ueno K, Saito R, Palacios T, Kong J, Dresselhaus MS. Large-area synthesis of high-quality uniform few-layer MoTe$_2$. J Am Chem Soc. 2015;137(37):11892.

72. Manzeli S, Allain A, Ghadimi A, Kis A. Piezoresistivity and strain-induced band gap tuning in atomically thin MoS$_2$. Nano Lett. 2015;15(8):5330.

73. Song S, Keum DH, Cho S, Perello D, Kim Y, Lee YH. Room temperature semiconductor-metal transition of MoTe$_2$ thin films engineered by strain. Nano Lett. 2016;16(1):188.

74. Mcdonnell S, Addou R, Buie C, Wallace RM, Hinkle CL. Defect-dominated doping and contact resistance in MoS$_2$. ACS Nano. 2014;8(3):2880.

75. Keum DH, Cho S, Kim JH, Choe DH, Sung HJ, Kan M, Kang H, Hwang JY, Kim SW, Yang H, Chang KJ, Lee YH. Bandgap opening in few-layered monoclinic MoTe$_2$. Nature Phys. 2015;11(6):482.

76. Cho S, Kim S, Kim JH, Zhao J, Seok J, Keum DH, Baik J, Choe DH, Chang KJ, Suenaga K, Kim SM, Lee YH, Yang H. Phase patterning for ohmic homojunction contact in MoTe$_2$. Science. 2015;349(6248):625.

77. Zhou L, Zubair A, Wang ZQ, Zhang X, Ouyang FP, Xu K, Fang WJ, Ueno K, Li J, Palacios T, Kong J, Dresselhaus MS. Synthesis of high-quality large-area homogenous 1T′ MoTe$_2$ from chemical vapor deposition. Adv Mater. 2016;28(43):9526.

78. Zhu JQ, Wang ZC, Yu H, Li N, Zhang J, Meng JL, Liao MZ, Zhao J, Lu XB, Du LJ, Yang R, Shi DX, Jiang Y, Zhang GY. Argon plasma induced phase transition in monolayer MoS$_2$. J Am Chem Soc. 2017;139(30):10216.

79. Lin YC, Dumcenco DO, Huang YS, Suenaga K. Atomic mechanism of the semiconducting-to-metallic phase transition in single-layered MoS$_2$. Nat Nanotech. 2014;9(5):391.

80. Li Y, Duerloo KA, Wauson K, Reed EJ. Structural semiconductor-to-semimetal phase transition in two-dimensional materials induced by electrostatic gating. Nat Commun. 2016;7:10671.

81. Zhang CX, Kc S, Nie YF, Liang CP, Vandenberghe WG, Longo RC, Zheng YP, Kong FT, Hong S, Wallace RM, Cho K. Charge mediated reversible metal-insulator transition in monolayer MoTe$_2$ and W$_x$Mo$_{1-x}$Te$_2$ Alloy. ACS Nano. 2016;10(8):7370.

82. Wang Y, Xiao J, Zhu HY, Li Y, Alsaid Y, Fong KY, Zhou Y, Wang SQ, Shi W, Wang Y, Zettl A, Reed EJ, Zhang X. Structural phase transition in monolayer MoTe$_2$ driven by electrostatic doping. Nature. 2017;550(7677):487.

83. Zhang F, Zhang HR, Krylyuk S, Milligan CA, Zhu YQ, Zemlyanov DY, Bendersky LA, Burton BP, Davydov AV, Appenzeller J. Electric-field induced structural transition in vertical MoTe$_2$- and Mo$_{1-x}$W$_x$Te$_2$-based resistive memories. Nat Mater. 2019;18(1):55.

Dr. Jinliang Wang is a professor at the Department of Physics, Beihang University. He received his BSc (1986), MSc (1994), and PhD (1998) honors in physics from Okayama University, Japan. His research focuses on the preparation of transition metal silicide thin film by solid phase reaction. He then pursued postdoctoral studies at the School of Science, Beihang University, in 1998. His research focuses on the characterization of doped hydrogenated nanocrystalline silicon films prepared by chemical vapor deposition. He was promoted as an associate professor in 2000 and a professor in 2006 at the Department of Physics, Beihang University. His current research interests involve low-dimensional physics, surface and film physics and semiconductor optics.

Dr. Yongji Gong is currently a professor in the Department of Materials Science and Engineering, Beihang University. He received his BS degree (2011) in chemistry from Peking University and PhD degree (2015) in chemistry from Rice University. Before he joined Beihang University, he worked as postdoctoral fellow in the Department of Materials Science and Engineering in Stanford University (2016-2017). His scientific interest is focused on the controllable